RSC Advances

PAPER

View Article Online
View Journal | View Issue

Cite this: *RSC Adv.*, 2015, **5**, 87723

A facile cosolvent/chelation method for the preparation of semi-crystalline $CuCl_2$(ethylene glycol)/poly(3-hexylthiophene) complexes displaying specific luminescence properties

Fang-Hsien Lu,[a] Mohamed Gamal Mohamed,[b] Tzeng-Feng Liu,[a] Chuen-Guang Chao[a] and Shiao-Wei Kuo*[bc]

Received 13th September 2015
Accepted 9th October 2015

DOI: 10.1039/c5ra18751f

www.rsc.org/advances

Semi-crystalline $CuCl_2$(ethylene glycol)/poly(3-hexylthiophene) complexes (CE–P3HT) with specific textures and self-assembled structures can be fabricated using a facile co-solvent/chelation method. The morphologies and self-assembled structures of these CE–P3HT complexes were dependent on the concentration of $CuCl_2$(ethylene glycol) ($CuCl_2$EG) in solution. Transmission electron microscopy (TEM) revealed the CE–P3HT sample comprising EG and numerous $CuCl_2$/P3HT dots (C–P3HT dots) that originated from the P3HT main chains interacting with $CuCl_2$ crystals; the average size of this C–P3HT dots was *ca.* 20 nm. Prior to formation of the solid state of CE–P3HT structures, the CE–P3HT complex in solution displayed a novel phenomenon: a specific luminescence property with an absorption energy gap of 3.71–4.46 eV. This quantum effect resulted from the chelates formed between the Cu^{2+} ions and the thioether units of the conjugated P3HT polymer.

Introduction

Nanoscale organic/metallic complexes have received much attention in the last decade due to their potential applications in photoelectric and magnetic devices, with their physical properties (conduction, luminescence, and mechanical behaviour) varying dramatically as a result of quantum effects.[1–5] Typically, such research has been performed using silver nanowire films, which possess a low resistance coefficient of 2×10^{-7} Ω cm.[6] The quantum effects and specific luminescence in these types of materials are generally supplied through the application of III–V and II–IV semiconductive nanocomposites (*e.g.*, GaAs, InP, CdSe, ZnS, ZnSe),[7–10] which must be fabricated under rigorous conditions (*e.g.*, high vacuum or elevated temperatures).[11–13]

In this study, we explored a surprisingly specific quantum effect that is derived from chelation of the conjugated polymer poly(3-hexlthiophene) (P3HT) with Cu^{2+} ions. When we prepared this P3HT chelation system in a polar solvent [*e.g.*, ethylene glycol (EG) and deionized water] it exhibited high luminous efficiency. P3HT is a well-established luminous and conductive material that is widely used in the fabrication of organic light emitting diodes (OLEDs) and organic photovoltaic (OPV) devices.[14–16] The quantum efficiency of P3HT is generally higher than that of poly(*N*-vinylcarbazole) (PVK),[17,18] but lower than those of other common fluorescent materials {*e.g.*, polyfluorene (PFO),[19,20] poly[2-methoxy-5-(2-ethyl-hexyloxy)-1,4-phenylene-vinylene] (MEH-PPV)[21,22]}; the quantum efficiency of P3HT can be increased, however, through blending with III–V and II–IV nanoparticles.[23–25] Although P3HT is almost always required for practical hole transfer applications, active emitting materials derived from P3HT and its derivatives are relatively rare.[26,27] In this study, we developed an excellent emission system formed from P3HT chelates and fabricated using a simple co-solvent method. This P3HT chelate is quite stable in the solid state under ambient air and can be dispersed evenly in solution.

Experimental procedure

Materials

Copper dichloride ($CuCl_2$) and ethylene glycol (EG, $C_2H_6O_2$) were purchased from Alfa Aesar and J. T. Baker, respectively. P3HT (M_n = 19 235; PDI = 2.055) was prepared according to procedures described in the literature.[28–30] Briefly, a solution of 3-hexylthiophene ($C_{10}H_{16}S$, 5 g) in $CHCl_3$ was cooled to −20 °C and then anhydrous iron trichloride ($FeCl_3$, 2 g) was added; this mixture was stirred for 12 h at room temperature; the solids

[a]*Department of Materials Science and Engineering, National ChiaoTung University, Hsinchu 300, Taiwan*

[b]*Department of Materials and Optoelectronic Science, Center for Functional Polymers and Supramolecular Materials, National Sun Yat-Sen University, Kaohsiung, 804, Taiwan*

[c]*School of Chemical Engineering, East China University of Science and Technology, Shanghai, China. E-mail: kuosw@faculty.nsysu.edu.tw*

were filtered vacuum, purified through Soxhlet extraction, and dried at 60 °C.

$CuCl_2$(ethylene glycol)/poly(3-hexylthiophene) complexes (CE–P3HT)

Solution I: $CuCl_2$ (1, 2, 4, 8, or 10 g) dissolved in EG at a concentration of 250–4000 ppm. Solution II: P3HT (10 or 40 mg) dissolved in toluene at a concentration of 1–4 wt%. Complex solutions were prepared after blending solutions I and II using the co-solvent method. Each resulting complex solution was ultrasonicated for 20 min at 40 °C, stirred for 12 h at 160 °C under argon, filtered, and centrifuged several times. Finally, the complex solution (1 mL) was placed on quartz glass (diameter: 2.5 cm) and heated at 100 °C to form a semi-crystalline CE–P3HT complex.

Characterization

X-ray diffraction (XRD) data were collected using a Bruker D8 DISCOVER apparatus. A rotating copper target was employed to obtain a monochromated incident beam having a wavelength (λ) of 1.5412 Å. The morphologies and shapes of the nanomaterials were observed through field emission scanning electron microscopy (FE-SEM), using a JSM-7000F microscope (JEOL, Japan), and optical microscopy (OM), using an Olympus BX51-P microscope. The chemical composition of the as-prepared surface was investigated using X-ray photoelectron spectroscopy (XPS, Thermo Scientific K-Alpha). Transmission electron microscopy (TEM, JEOL 2100-F) was performed at an accelerating voltage of 200 kV. The energy levels of the CE–P3HT complex were measured through UV-Vis-NIR spectrophotometry (Hitachi U-4100).

Results and discussion

XRD patterns and morphologies of CE–P3HT complexes

Table 1 lists all of the CE–P3HT samples that we synthesized from 1 wt% P3HT and various concentrations of $CuCl_2$EG. As revealed in Fig. 1, the XRD pattern of pure P3HT featured a broad amorphous peak at values of θ in the range from 22 to 31°. In addition, the sharp crystalline peaks obtained in the XRD pattern of $CuCl_2$ were absent in the diffraction patterns of the CE–P3HT complexes, suggesting that the $CuCl_2$ structure was destroyed in the presence of P3HT. The XRD patterns of the CE–P3HT samples A–D revealed only amorphous phases;

Table 1 The *d*-spacing of semi-crystalline of CE–P3HT

CE–P3HT sample	Concentration of $CuCl_2$EG (ppm)	Concentration of P3HT (wt%)	*d*-spacing of CE–P3HT (nm)
Pure P3HT	0	1	0.202
A	250	1	0.199
B	500	1	0.196
C	1000	1	0.156
D	2000	1	0.152
E	4000	1	0.160

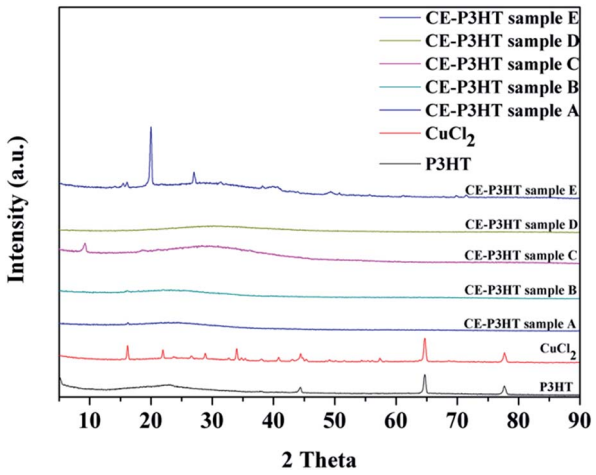

Fig. 1 The X-ray spectra of semi-crystalline CE–P3HT samples.

we observed, however, that $CuCl_2$ crystals had precipitated in CE–P3HT sample E, a result of the high concentration of its precursor $CuCl_2$EG solution. And the poor compatibility between $CuCl_2$ and P3HT. The *d*-spacing of P3HT decreased generally upon increasing the CE concentration in the CE–P3HT complexes, due to chelation between the Cu ions and the thioether units; in other words, chelation decreased the distance between the chains of P3HT.

Fig. 2 presents OM images of the morphologies and textures of the CE–P3HT samples. Those possessing amorphous

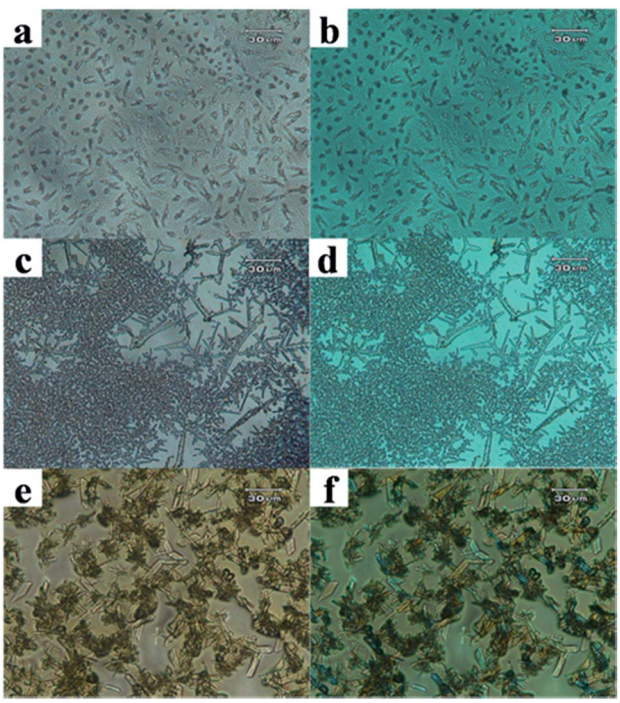

Fig. 2 OM images of semi-crystalline CE–P3HT samples, (a) sample C and (b) texture polarized light of sample C, (c) sample D and (d) texture polarized light of sample D, and (e) sample E and (f) texture polarized light of sample E.

structures could offer semi-opaque and specific textures, resulting from the presence and even dispersion of P3HT in the samples. Moreover, the CE–P3HT complexes exhibited a capacity for self-assembly. Indeed, rod-like structures [Fig. 2(a) and (b)] transformed into branch-like [Fig. 2(c) and (d)] and silk-like [Fig. 2(e) and (f)] structures upon controlling of synthesis conditions, namely by increasing the concentration of the $CuCl_2$EG solution. SEM and energy dispersive spectroscopy (EDS) provided evidence for the presence of CE–P3HT, confirming the formation of chelated structures. Although we synthesized the CE–P3HT samples using a slight P3HT, the signal of the sulfur atoms remained evident (Fig. 3).

According to these results and crystallography concepts, all of the different types of CE–P3HT structures were built on a similar crystalline system, as evidenced by the existence of approximate *d*-spacing. For example, both copper (Cu) and gold (Au) metal have face-centered cubic (FCC) structures and the same packing efficiency of 0.7405, even though they possess different atomic radii and volumes: Cu (radius (*r*): 128 ppm; volume: 4.745×10^{-29} m^3), Au (*r*: 144 ppm; volume: 6.757×10^{-29} m^3). Furthermore, introducing the equation for the *d*-spacing of an FCC structure, its atomic packing factor could be described as

$$\frac{N_{\text{Atoms}} V_{\text{Atom}}}{V_{\text{Unitcell}}} = \frac{6\frac{4}{3}\pi r^3}{(16r^3)\frac{3\sqrt{3}}{2}\sqrt{\frac{2}{3}}}$$

where *r* is the atomic radius and the simplification $d^3 \propto a^3$, r^3 could be identified in the same crystalline plane as (111); hence, the structural model of the CE–P3HT complexes is based on the frame of π–π stacking as that of P3HT.

TEM analyses of the self-assembled structures formed from the CE–P3HT complexes

Although XRD and EDS analyses confirmed the components and structures of the CE–P3HT complexes, the dispersion of P3HT in CE–P3HT remained related to the formation of an amorphous structure. We used TEM analysis to identify this phenomenon (Fig. 4). We observed several dots dispersed uniformly in CE–P3HT samples C and E, with the average size of the dots (named C–P3HT) being approximately 20 nm. At this size, polymer dot effects[31–34] and carbon dot effects[35,36] would appear, with the energy level of the highest occupied molecular orbital (HOMO) and lowest unoccupied molecular orbital (LUMO) of P3HT both increasing simultaneously as a result of decreased conjugation of P3HT upon chelation. Fig. 5 displays the corresponding photoluminescence phenomenon of the C–P3HT dots dispersed in the complex solution exposed to a UV lamp. The blue fluorescence observed in this complex solution was different from the fluorescence of pure P3HT. In addition, the complex solution exhibited the greatest fluorescence (Fig. 6) when the highest number of C–P3HT dots was present in the

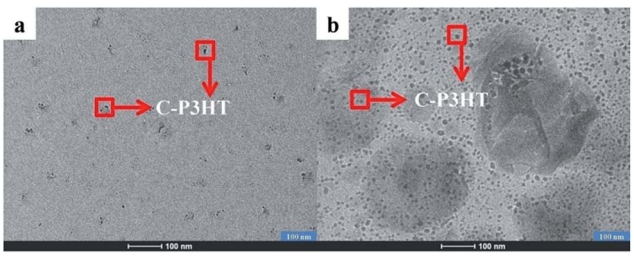

Fig. 4 TEM images of C–P3HT, derived from (a) CE–P3HT sample C, and (b) CE–P3HT sample E.

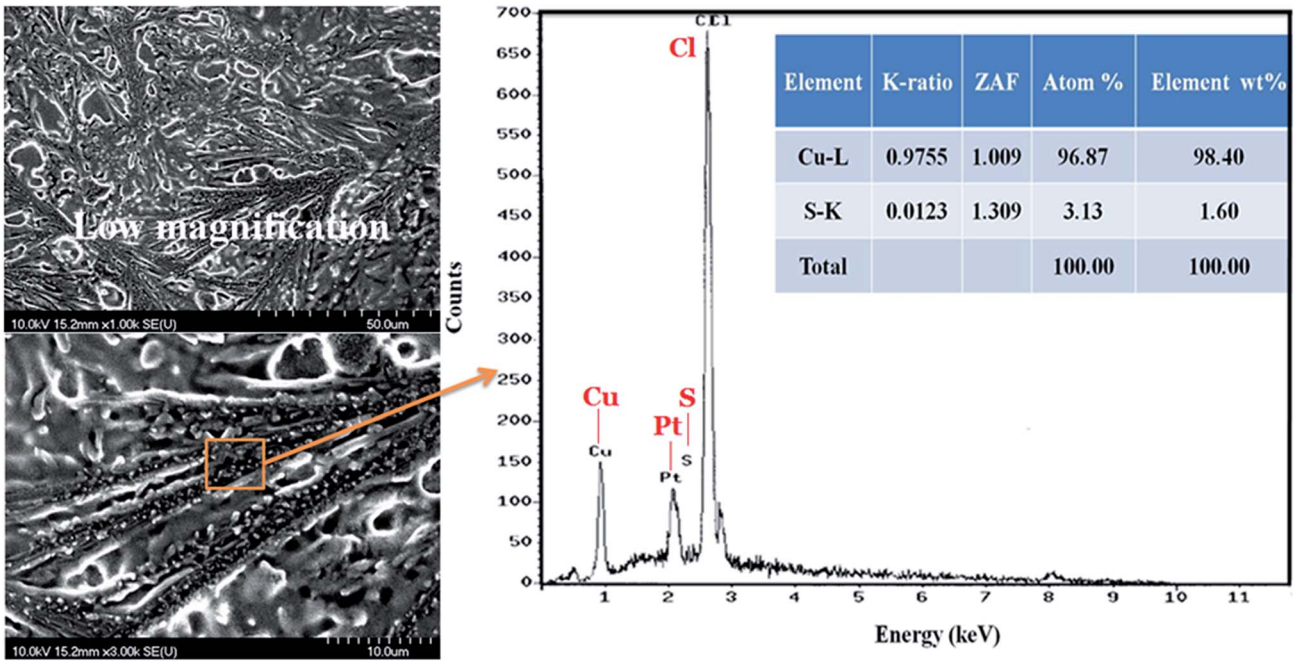

Fig. 3 The SEM and EDS images of semi-crystalline CE–P3HT sample C.

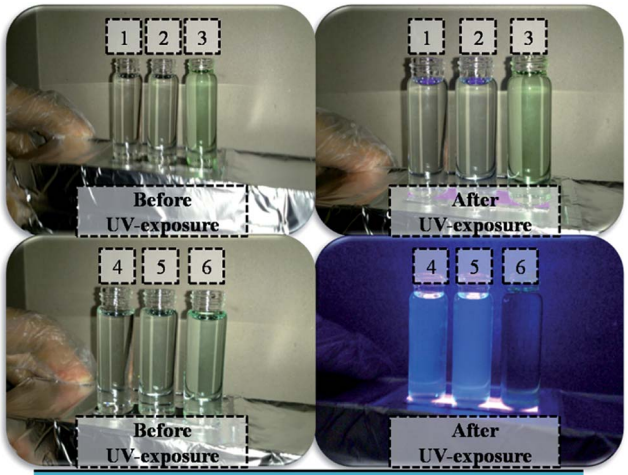

Solution No.	Components of complex solution
1	$CuCl_2$ ethylene glycol (1000 ppm)
2	$CuCl_2$ ethylene glycol (2000 ppm)
3	$CuCl_2$ ethylene glycol (4000 ppm)
4	$CuCl_2$ ethylene glycol (1000 ppm)/P3HT (1 wt%)
5	$CuCl_2$ ethylene glycol (2000 ppm)/P3HT (1 wt%)
6	$CuCl_2$ ethylene glycol (4000 ppm)/P3HT (1 wt%)

Fig. 5 Photographs of complex solutions and pure $CuCl_2EG$ solutions under with and without UV illumination (wavelength: 254 nm).

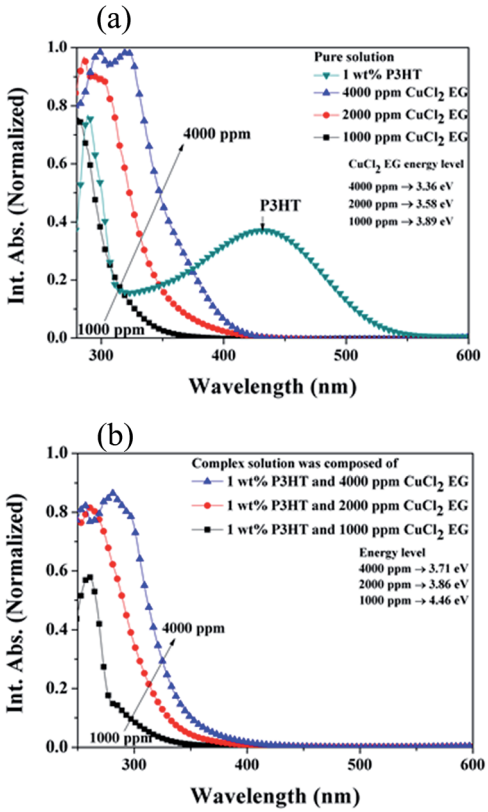

Fig. 7 (a) Absorptions of complex solutions and (b) absorptions of pure $CuCl_2EG$ and P3HT solutions.

complex solution (derived from the blending of 250 ppm $CuCl_2$ with 4 wt% P3HT); to understand the cause of this specific fluorescence, which resulted from changes in the band gap of P3HT, we recorded the absorption spectra of the complex solutions [Fig. 7(a)]. Clearly, the absorption of P3HT (431 nm) disappeared after blending with $CuCl_2EG$, with the band gap of the complex solution (calculated using the expression $E_g = 1240/\lambda_g$ where E_g is energy gap and λ_g is wavelength of absorption) being greater than those of the original pure $CuCl_2EG$

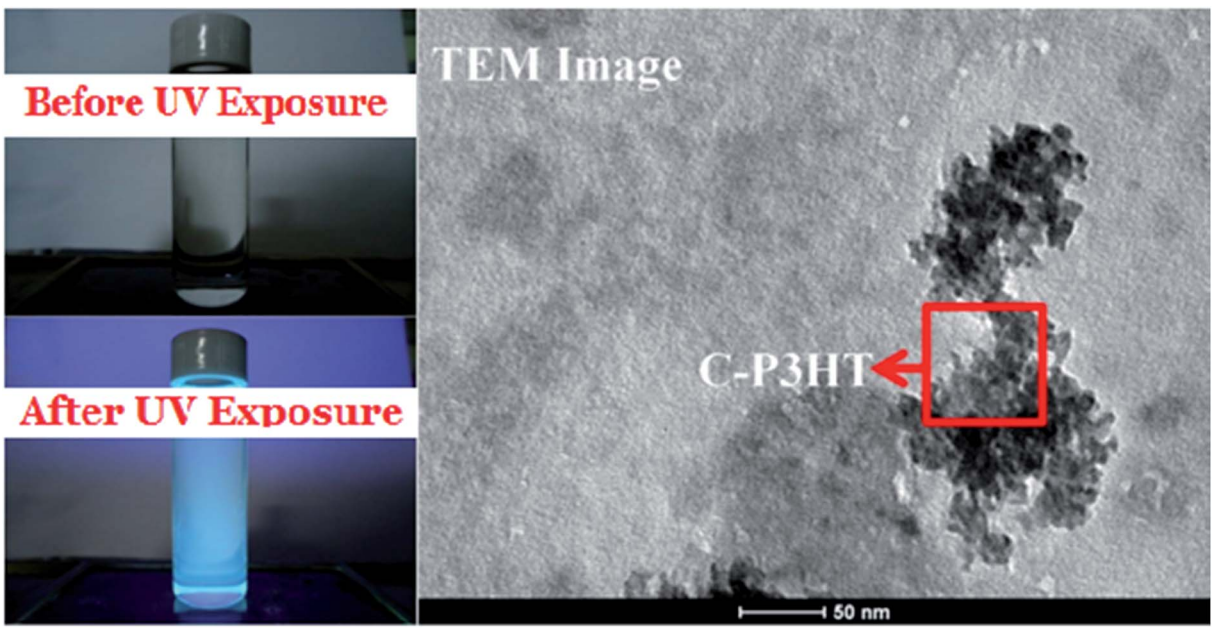

Fig. 6 The phenomenon of dispersed C–P3HT in complex solution and semi-crystalline CE–P3HT F, formed with 250 ppm $CuCl_2EG$ and 4 wt% P3HT.

and P3HT solutions [Fig. 7(b)]. Specifically, the formation of C–P3HT involved the transfer of electron density from the HOMO of P3HT to the atomic orbital of the copper ions in the presence of UV. The increasing that occurred in the band gaps of the complex solutions synthesized at lower concentrations of $CuCl_2$EG were due to the self-property of $CuCl_2$EG. Typically, a blue-shift generally represents the luminescence occurring at a shorter wavelength.

The C–P3HT dots were formed from $CuCl_2$ and P3HT through Cu–S chelation; this chelation, corresponding to a coordination complex, would, however, affect the charge transfer process. The increases in the band gaps of the complex solutions were derived from changes in the sizes of the C–P3HT dots. The smaller C–P3HT dots in the complex solution prepared from 1000 ppm $CuCl_2$ and 1 wt% P3HT displayed a band gap of 4.46 eV. The C–P3HT dots featured various morphologies of their P3HT chains. Therefore, the band gaps of the complex solutions were affected by Cu–S chelation and the sizes of the C–P3HT dots. Variations in the $CuCl_2$ concentration and the Cu–Cl coordination structure in EG affected the absorption of pure $CuCl_2$EG in the presence of UV. In solution, $CuCl_2$ could undergo self-absorption, due to its Cu ions; thus, $CuCl_2$EG possessed optical absorption at wavelengths in the range 300–400 nm. Fig. 8 presents the luminescence properties of the complex solutions as determined from PL spectra. The luminescence wavelengths of the complex solutions all were located in the region from 450 to 505 nm; these wavelengths are shorter than that of the luminescence from the pure P3HT solution [Fig. 8(a)]. Moreover, high luminescence intensity appeared from the complex solution derived from blending with 1000 ppm $CuCl_2$ and 1 wt% P3HT. This phenomenon is consistent with the results displayed in Fig. 5 and 8(b). Fig. 9 presents a possible structure for the chelated C–P3HT dots dispersed in the complex solution. In the PL spectrum, the intensity of 0-1 singlet state was stronger in the complex solution derived from 1000 ppm of $CuCl_2$ and 1 wt% of P3HT in EG, due to P3HT self-aggregation, this low concentration of $CuCl_2$ (1000 ppm) could not disrupt the self-aggregation of the P3HT chains. In comparison, in CE–P3HT sample E, the presence of $CuCl_2$ at 4000 ppm in EG led to complete disruption of the aggregated polymer chains, because of the lower relative concentration with P3HT/$CuCl_2$ in EG. At same time, the deconstructive models of π–π stacking of P3HT did not form in the complex solution; therefore, it tended to exhibit high luminescence (in the presence of $CuCl_2$ at 1000 ppm), with the intensity of the 0-0 singlet state being distinctly stronger than the other. The energy transfer occurred from the 0-0 to 0-1 singlet state through self-aggregation of the P3HT chains, such that the intensity of the 0-1 singlet state was higher than that of the 0-0 singlet state. Therefore, the changes in the band gaps and luminescence wavelengths both derived from Cu–S chelation, whereas the luminescence intensities were affected by changes in the P3HT microstructures. We observed another interesting phenomenon in the UV-Vis spectra, where the change in the band gap was obvious in the complex solution formed from 1000 ppm of $CuCl_2$ and 1 wt% of P3HT in EG. This phenomenon derived from the smaller conjugated length of P3HT upon dissolving and dispersing in EG *via* Cu–S chelation. The lower concentration of $CuCl_2$EG interacted with the shorter chains of P3HT; a higher concentration of $CuCl_2$EG of 4000

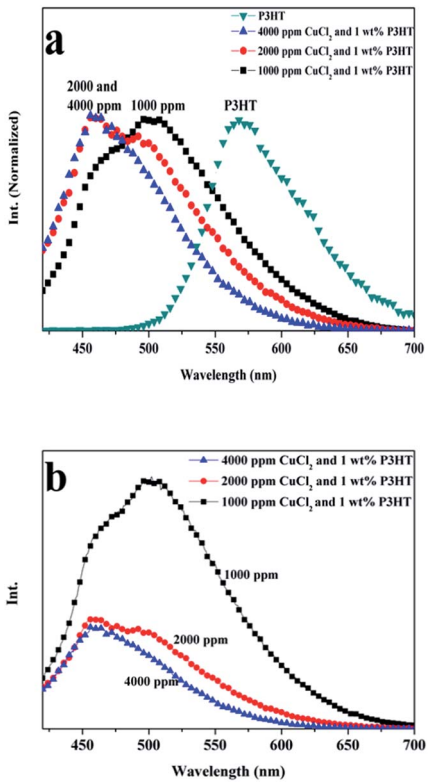

Fig. 8 The luminescence of complex solutions, (a) normalized intensity, (b) relative intensity.

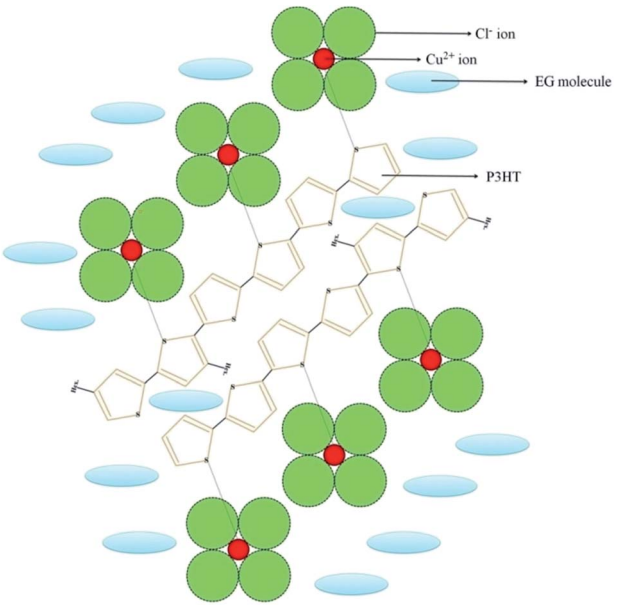

Fig. 9 Structural model of the C–P3HT dots dispersed in the complex solution.

ppm resulted in the longer chains of P3HT being dispersed in this blending system.

Structural model of CE–P3HT complexes

Fig. 10 illustrates the structure of the C–P3HT dots in solution, but the model of the C–P3HT dots in CE–P3HT was quite different. XRD patterns and TEM analyses confirmed that CE–P3HT was formed with C–P3HT and EG, and that the CE–P3HT structure was built on the model of π–π stacking of P3HT, as displayed in Fig. 10(b). Specifically, the $CuCl_2$ lattices were inserted between the chains of P3HT, while the C–P3HT dots formed in the CE–P3HT structure, and the C–P3HT dots were dispersed evenly in the EG phase. In other words, the structure of $CuCl_2$, which has a rhombohedral lattice system as presented in Fig. 10(a), was disrupted upon chelation to the soft material P3HT. The reference of Cu(I) chelated poly-alkoxythiophene. Hence using in the OPV would support the CE–P3HT structure formation,[37,38] an amorphous structure appeared in CE–P3HT. $[CuCl_4]^{2-}$, possessing a planar structure, was presumably the main type of Cu–Cl coordination complex formed in the solution. The cupric ion, in the form of $[CuCl_4]^{2-}$, was bound by the lone pair of electrons of a C–S–C unit after blending of $CuCl_2$EG and P3HT. Fig. 10 also displays the possible structure of the chelated C–P3HT, formed from $[CuCl_4]^{2-}$ and P3HT in the complex solution.

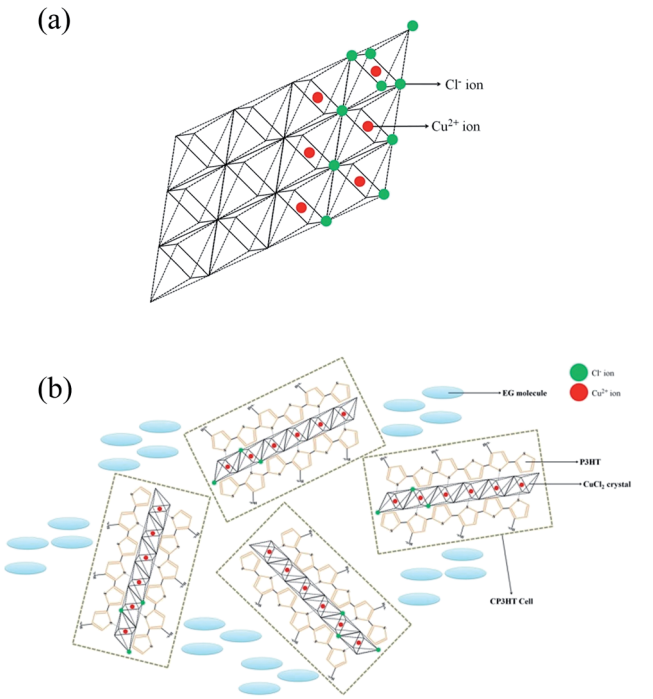

Fig. 10 (a) Solid state structure with $CuCl_2$; Cl^- ions occupying corner sites and Cu^{2+} ions occupying interstitial sites. (b) Illustration of the C–P3HTdots dispersed in CE–P3HT.

To confirm this structure, we use the TEM analyses as shown in Fig. 11. Clearly, the triangle morphologies are presented and derived from $CuCl_2$ rhombic structure. Moreover, the triangle structure is similar to core/shell structure and we supposed the core formed with $CuCl_2$ and CuCl, and the shell possessing the semi-transparent morphology was composed of P3HT and EG. We prove this structure by using electron beam voltage (200 kV) to focus the sample on the one position until the complex melting. When the core/shell structure was melted after 1 second, the shell organization was move around. After 5 second, the core and shell organizations had been separated obviously. In the TEM normal opinion, the soft material (polymer), which is like shell organization, can be melted and moved under electron focus beam and high temperature. Moreover, the electron beam can easily transmit the soft material; therefore, the shell images were more transparent than core.

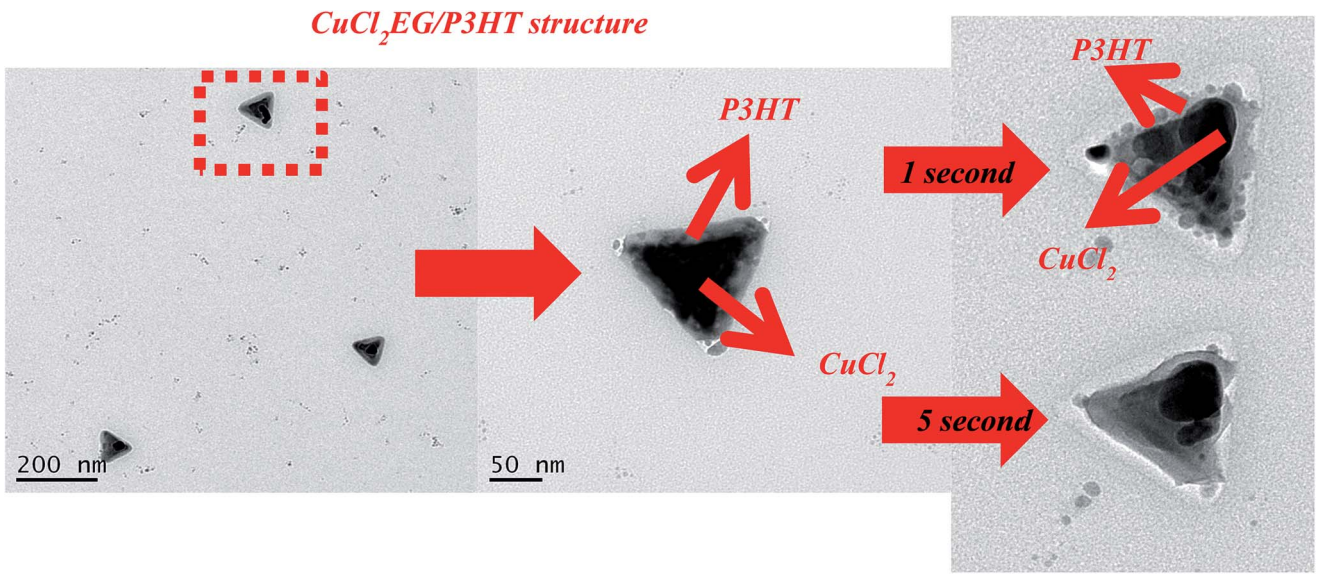

Fig. 11 TEM images of $CuCl_2$EG/P3HT structure after 1 and 5 second electron beam.

Conclusions

We have employed a co-solvent method and the chelation behaviour of thioethers, Cu^{2+}, and Cl^{-} ions to prepare a series of semi-crystalline CE–P3HT complexes and CE–P3HT complex solutions. The CE–P3HT complex solution exhibited a specific luminescence, different from that of pure P3HT. The semi-crystalline CE–P3HT complex was amorphous, capable of self-assembly. TEM analyses confirmed that the semi-crystalline CE–P3HT complex was composed of EG and numerous C–P3HT dots. The average size of the C–P3HT dots (*ca.* 20 nm) could be controlled by varying the $CuCl_2$EG concentration. Moreover, P3HT could be dissolved and dispersed in $CuCl_2$EG solutions to form new coordination complexes and a material displaying a specific luminescence.

Acknowledgements

This study was supported financially by the Ministry of Science and Technology, Republic of China, under contracts MOST 100-2221-E-110-029-MY3 and MOST 102-2221-E-110-008-MY3. We also thank Mr Hsien-Tsan Lin of the Regional Instruments Center at National Sun Yat-Sen University for helping with the TEM experiments.

References

1 L. Lou, K. Yu, Z. L. Zhang, B. Li, J. Z. Zhu, Y. T. Wang, R. Huang and Z. Q. Zhu, *Nanoscale*, 2011, **3**, 2315.
2 L. Hu, R. R. Zhang and Q. W. Chen, *Nanoscale*, 2014, **6**, 14064.
3 M. Hu, A. A. Belik, M. Imura and Y. Yamauchi, *J. Am. Chem. Soc.*, 2013, **135**, 384.
4 H.-Y. Lian, M. Hu, C.-H. Liu, Y. Yamauchi and K. C.-W. Wu, *Chem. Commun.*, 2012, **48**, 5151.
5 M. Hu, S. Furukawa, R. Ohtani, H. Sukegawa, Y. Nemoto, J. Reboul, S. Kitagawa and Y. Yamauchi, *Angew. Chem., Int. Ed.*, 2012, **51**, 984.
6 S. de, T. M. Higgins, P. E. Lyons, E. M. Doherty, P. N. Nirmalraj, W. J. Blau, J. J. Boland and J. N. Coleman, *ACS Nano*, 2009, **3**, 1767.
7 N. Tomczak, R. R. Liu and J. G. Vancso, *Nanoscale*, 2013, **5**, 12018.
8 N. Mastour, Z. B. Hamed, A. Benchaabane, M. A. Sanhoury and F. Kouki, *Org. Electron.*, 2013, **14**, 2093.
9 H.-C. Zhang, X. W. Du, Y. Q. Wang, Q. M. Guan, Y. M. Sun, Y. P. Cui and J. Y. Zhang, *Phys. E*, 2013, **49**, 1.
10 N. Fuke, L. B. Hoch, A. Y. Koposov, V. W. Manner, D. J. Werder, A. Fukui, N. Koide, H. Katayama and M. Sykora, *ACS Nano*, 2010, **4**, 6377.
11 O. I. Micic, C. J. Curtis, K. M. Jones, J. R. Sprague and A. J. Nozik, *J. Phys. Chem.*, 1994, **98**, 4966.
12 J. M. Nedeljkovic, O. I. Micic, S. P. Ahrenkiel, A. Miedaner and A. J. Nozik, *J. Am. Chem. Soc.*, 2004, **126**, 2632.
13 H. S. Chen, B. Lo, J. Y. Hwang, G. Y. Chang, C. M. Chen, S. J. Tsai and S. J. J. Wang, *J. Phys. Chem. B*, 2004, **108**, 17119.
14 J. Huang, Z. G. Yin and Q. D. Zheng, *Energy Environ. Sci.*, 2011, **4**, 3861.
15 K. Yao, C. Liu, Y. W. Chen, L. Chen, F. Li, K. Liu, R. X. Sun, P. S. Wang and C. H. Yang, *J. Mater. Chem.*, 2012, **22**, 7342.
16 Y. X. Liu, M. A. Summers, C. Edder, J. M. J. Frechet and M. D. McGehee, *Adv. Mater.*, 2005, **17**, 2960.
17 C. Jiang, W. Yang, J. B. Peng, S. Xiao and Y. Cao, *Adv. Mater.*, 2004, **16**, 537.
18 E. L. Williams, K. Haavisto, J. Li and G. E. Jabbour, *Adv. Mater.*, 2007, **19**, 197.
19 M. Ariu, D. G. Lidzey, M. Sims, A. J. Cadby, P. A. Lane and D. D. C. Bradley, *J. Phys.: Condens. Matter*, 2002, **14**, 9975.
20 T. Virgili, D. G. Lidzey and D. D. C. Bradley, *Synth. Met.*, 2000, **111–112**, 203.
21 J. C. de Mello, H. F. Wittmann and R. H. Friend, *Adv. Mater.*, 1997, **9**, 230.
22 Y. Cao, I. D. Parker, G. Yu, C. Zhang and A. J. Heeger, *Nature*, 1999, **397**(4), 414.
23 M. J. Greaney, S. Das, D. H. Webber, S. E. Bradforth and R. L. Brutchey, *ACS Nano*, 2012, **6**, 4222.
24 M. Schierhorn, S. W. Boettcher, J. H. Peet, E. Matioli, G. C. Bazan, G. D. Stucky and M. Moskovits, *ACS Nano*, 2010, **4**, 6132.
25 H. C. Liao, S. Y. Chen and D. M. Liu, *Macromolecules*, 2009, **42**, 6558.
26 B. Xu and S. Holdcroft, *Macromolecules*, 1993, **26**, 4457.
27 N. Banerji, S. Cowan, E. Vauthey and A. J. Heeger, *J. Phys. Chem. C*, 2011, **115**, 9726.
28 R. D. McCullough, R. D. Lowe, M. Jayaraman and D. L. Anderson, *J. Org. Chem.*, 1993, **58**, 904.
29 F. Tassinari, E. Tancini, M. Innocenti, L. Schenetti and C. Fontanesi, *Langmuir*, 2012, **28**, 15505.
30 M. A. Ibrahim, B. G. Lee, N. G. Park, J. R. Pugh, D. D. Eberl and A. J. Frank, *Synth. Met.*, 1999, **105**, 35.
31 W. Sun, S. Hayden, Y. H. Jin, Y. Rong, J. B. Yu, F. M. Ye, Y. H. Chan, M. Zeigler, C. F. Wu and D. T. Chiu, *Nanoscale*, 2012, **4**, 7246.
32 L. Wei, P. Zhou, Q. X. Yang, Q. Y. Yang, M. Ma, B. Chen and L. H. Xiao, *Nanoscale*, 2014, **6**, 11351.
33 D. Tuncel and H. V. Demir, *Nanoscale*, 2010, **2**, 484.
34 Y. Q. Li, J. Liu, B. Liu and N. Tomczak, *Nanoscale*, 2012, **4**, 5694.
35 W. Q. Kong, J. Liu, R. H. Liu, H. Li, Y. Liu, H. Huang, K. Y. Li, J. Liu, S. T. Lee and Z. H. Kang, *Nanoscale*, 2014, **6**, 5116.
36 Z. Yang, M. H. Xu, Y. Liu, F. J. He, F. Gao, Y. J. Su, H. Wei and Y. F. Zhang, *Nanoscale*, 2014, **6**, 1890.
37 I.-C. Wu, C.-H. Lai, D.-Y. Chen, C. W. Shih, C.-Y. Wei, B.-T. Ko, C. Ting and P.-T. Chou, *J. Mater. Chem.*, 2008, **18**, 4297.
38 E. Zaminpayma, *Comput. Mater. Sci.*, 2013, **75**, 24.